https://doi.org/10.5194/cp-2023-71
Preprint. Discussion started: 15 September 2023

Climate of the Past Discussions

Tracing seasonal signals in dry/wet status for regions with simultaneous rain and heat from Eastern and Central Asia since the Last Glacial Maximum

Simin Peng[1], Yu Li[1*], Zhansen Zhang[1], Mingjun Gao[1], Xiaowen Chen[1], Junjie Duan[1], Yaxin Xue[1]

[1]*Key Laboratory of Western China's Environmental Systems (Ministry of Education), College of Earth and Environmental Sciences, Center for Hydrologic Cycle and Water Resources in Arid Region, Lanzhou University, China*

[*]Corresponding author

E-mail address: liyu@lzu.edu.cn (Y. Li).

Abstract

The global monsoon region with the summer precipitation regime and the Mediterranean climate region with the winter precipitation regime showed opposite dry/wet evolution since the Last Glacial Maximum (LGM). The remarkable difference in summer precipitation regime and winter precipitation regime reveal the seasonal signals of precipitation in multi-time scale climate change. Most studies revealed that the dry/wet status with the summer precipitation regime in Eastern and Central Asia (EA and CA) contradicted those with the winter precipitation regime in CA. Based on the comprehensive study of modern observation datasets, model outputs of eight

https://doi.org/10.5194/cp-2023-71
Preprint. Discussion started: 15 September 2023

climate models from the Paleoclimate Model Intercomparison Project phase 3 (PMIP3) and proxy records from EA and CA, here we show that seasonal signals of precipitation derived from the simultaneity of rain and heat periods could govern the difference and linkage in dry/wet status from EA and CA. EOF analysis results of mean annual precipitation uncover different precipitation regimes in EA and CA. However, the similarity between EA and the east of CA, indicated by EOF results of summer and winter precipitation, suggested seasonal signals of precipitation are the primary factor causing the linkage in dry/wet status at short-term timescales. In particular, summer and winter precipitation in EA and CA is associated with the Asian monsoon, westerlies, ENSO, NAO, and PDO. At long-term timescales, the compilation of 42 proxy records since the LGM in EA and CA reveals parallel dry/wet changes in EA and the east of CA as well, attributing to seasonal signals triggered by the insolation in different seasons. PMIP3 multi-model simulation between the LGM and Mid-Holocene (MH) in summer and winter visually was conducted to analyze paleoclimate mechanisms of difference and linkage in dry/wet status from EA and CA. Results show that summer insolation influences the meridional temperature gradient and sea level pressure in the summer, changing the intensity of the westerly winds and summer monsoon and further controlling the summer precipitation in EA and the east of CA. Meanwhile, winter insolation contributes to the general warming in EA and the core region of CA, and in turn results in lower relative humidity, which ultimately increases winter precipitation during the LGM. Overall, we suggest, in addition to the traditional difference caused by different precipitation regimes, that dry/wet status in EA and CA universally have

https://doi.org/10.5194/cp-2023-71
Preprint. Discussion started: 15 September 2023

Climate of the Past Discussions

inter-regional connections affected by seasonal signals of precipitation at multi-time scales.

Keywords

seasonal signals; Eastern Asia (EA); Central Asia (CA); dry/wet status; multi-time scales; Last Glacial Maximum

1 Introduction

As typical midlatitude climatic regions, Eastern and Central Asia (EA and CA) are commonly featured with vigorous circulations and are dominated by two atmospheric systems, namely midlatitude westerlies and Asian monsoon (Li, 1990; Zhang and Lin, 1992; Chen et al., 2008; Nagashima et al., 2011). These two regions are generally characterized by opposite climate and environment changes, embodied in water resources, vegetation cover and ecosystems, which gives rise to their different response to climate change (Sorg et al., 2012; Zhang and Feng, 2018). CA, where precipitation is scarce throughout the year, is the largest arid region in the mid-latitudes dominated by westerlies (Chen et al., 2009; Huang et al., 2015a). On the contrary, affected by the Asian summer monsoon that carries water vapor from the Ocean, the monsoon-dominated EA has more precipitation (Wang et al., 2017). Therefore, exploring spatiotemporal climate and environment changes in EA and CA has attracted much research interest.

Over the past few years, there have been many comparative studies for dry/wet

https://doi.org/10.5194/cp-2023-71
Preprint. Discussion started: 15 September 2023

changes at multi-time scales from EA and CA. Early works suggested that the climate change mode of 'cold-wet' or 'warm-dry' occurred in northwestern China during the last glacial/interglacial cycle, which is different from the 'cold-dry' or 'warm-wet' modes of the monsoon climate (Li, 1990; Han and Qu, 1992; Han et al., 1993). Based on the integration of paleoclimate records, modern meteorological observation data and paleoclimate simulations, Chen et al. (2008, 2009, 2019) revealed the 'westerlies-dominated climatic regime' in arid CA from millennium to interdecadal timescales, which is out-of-phase or anti-phased with the dry/wet status in the monsoon-dominated regions. However, the paleoclimate records in part regions of CA provided asynchronous climate evolution history, in contradiction with the dry/wet changes caused by the westerlies (An et al., 2006; Zhao et al., 2015; Wang et al., 2018). The latest studies proposed that the persistent weakening of the East Asian summer monsoon since 1958, causing an increasing contribution of the monsoonal water vapor transport, thereby enhancing summer precipitation in arid CA (Chen et al., 2021a; Chen et al., 2021b). Therefore, further research is needed to explain dry/wet changes in different regions and explore the difference and linkage in climate change modes from EA and CA at multi-time scales.

The seasonal signals of precipitation derived from the simultaneity of rain and heat periods, behaving as that the summer half-year at short-term timescales and warm period at long-term timescales has more precipitation than the winter half-year and cold period respectively, is an important phenomenon in climate change in EA and CA at the multi-time scale. This study aims to focus on the transitional zone in the arid and semi-

https://doi.org/10.5194/cp-2023-71
Preprint. Discussion started: 15 September 2023

arid region of eastern CA where the westerlies and the monsoon interact and have the summer precipitation regime the same as the monsoon-dominated EA. Utilizing modern observations, paleoclimate proxies, and model simulations, we conducted a comprehensive analysis for dry/wet status in EA and CA at multi-time scales based on seasonal signals of precipitation.

2 Materials and methods

2.1 Study area

CA is the largest arid and semi-arid areas in the mid-latitude hinterland of the Eurasian continent, extending from the Caspian Sea in the west to the modern Asian summer monsoon limit in the east, comprising the central Asian countries, NW China, and southern Mongolian Plateau (Fig. 1). Considering that the strength and trajectory of monsoon circulation is a major control on moisture in EA, we viewed the monsoon China in the east and south of the modern Asian summer monsoon limit as EA (Fig. 1). We calculated the precipitation difference between the summer (April, May, June, July, August, and September) and winter (January, February, March, October, November, and December) half year over 1971-2020, and then defined the region greater than 0 mm as the simultaneous region of rain and heat periods (Fig. 1, gray slash). Eastern CA belongs to the simultaneous region of rain and heat periods. The seasonality perspective implies that different precipitation regimes could affect the difference and linkage in climate change modes from EA and CA at the multi-time scale. Taking seasonal signals as the dividing criteria, the core region of CA is characterized by a wet cold-season

https://doi.org/10.5194/cp-2023-71
Preprint. Discussion started: 15 September 2023

climate, whereas EA and eastern CA is characterized by a wet warm-season climate (Fig. 1).

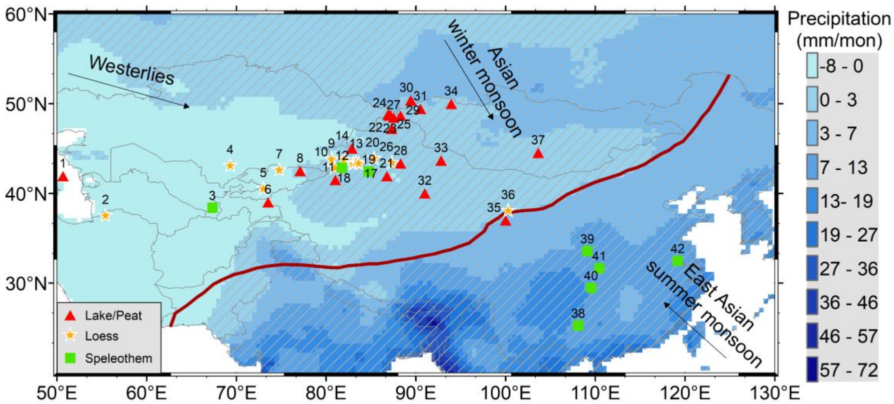

Figure. 1 Overview map showing the paleoclimate record sites selected in this study from EA and CA, the difference between summer and winter precipitation over 1965-2014 (shade), and the dominant circulation systems, including the westerlies, Asian winter monsoon and East Asian summer monsoon. The modern Asian summer monsoon limit (red solid line) is summarized by Chen et al. (2008, 2019). The gray slash represents the simultaneous region of the rain and heat periods.

2.2 Modern observation and analytical methods

The monthly high-resolution (0.5°×0.5°) land precipitation data (referred to as CRU TS4.06) are selected from a Climatic Research Unit (CRU) updated gridded climate dataset in the University of East Anglia (van der Schrier et al., 2013; Harris et al., 2014; Barichivich et al., 2021). The CRU monthly climate archives obtain from the auspices of the World Meteorological Organization (WMO) in league with the US National Oceanographic and Atmospheric Administration (NOAA, via its National Climatic Data Center, NCDC). Global Reanalysis 1 dataset including monthly mean geopotential height, zonal wind, and meridional wind is collected from the National Centers for Environmental Prediction/National Center for Atmospheric Research

https://doi.org/10.5194/cp-2023-71
Preprint. Discussion started: 15 September 2023

(NCEP/NCAR) (Kalnay et al., 1996). The reanalysis datasets have a horizontal resolution of 2.5° in latitude and longitude and a vertical resolution of 17 pressure levels from 1000 to 10 hPa. The high-resolution monthly averaged data high resolution for the vertical integral water vapor from the European Centre for Medium-Range Weather Forecasts (ECMWF) reanalysis v5 (ERA5), intending to be used as a meteorological forcing dataset for land surface and hydrological models, is used in this study. This dataset is from 1979 to the present with a spatial resolution of 0.25° in latitude and longitude and a single level integrated from the surface to the top of the atmosphere (Hersbach et al., 2020).

We used the National Centers for Environmental Information (NCEI) Pacific Decadal Oscillation (PDO) index based on NOAA's extended reconstruction of SSTs (ERSST Version 5) to analyze long-lived El Niño-like pattern of Pacific climate variability (Zhang et al. 1997; Mantua and Hare, 2002). The data can be obtained at https://www.ncei.noaa.gov/pub/data/cmb/ersst/v5/index/ersst.v5.pdo.dat. The Niño 3.4 index is the most commonly used index to define El Niño and La Niña events. We selected the Niño 3.4 of area-averaged SST from 5°S-5°N and 170-120°W using the HadISST1 dataset (Rayner et al., 2003). The data can be obtained at https://psl.noaa.gov/gcos_wgsp/Timeseries/Nino34/. Positive values of the North Atlantic Oscillation (NAO) index are typically associated with stronger midlatitude westerlies and increased water vapor content from the North Atlantic. We used the Hurrell NAO index (station-based) to investigate the impact factor of midlatitude westerlies (Hurrell, 1995; Hurrell and Deser, 2009). The data can be obtained at

https://doi.org/10.5194/cp-2023-71
Preprint. Discussion started: 15 September 2023

https://climatedataguide.ucar.edu/sites/default/files/2022-10/nao_station_monthly.txt.

Empirical orthogonal function (EOF) is a powerful method for dimensionality reduction and pattern extraction. EOF can decompose multidimensional climate data from different locations into spatial (EOF modes) and temporal functions (principal components). Therefore, to investigate the spatiotemporal variations of precipitation at the interannual timescale over EA and CA, the EOF analysis was applied to the CRU TS4.06 gridded precipitation data and ERA5 vertical integral water vapor. We focused on the first two leading modes that objectively account for the majority of dry/wet status in EA and CA (Lorenz, 1956).

2.3 Calculation of Monsoon and westerly wind index

The East Asian summer monsoon index (EASMI) is defined as the 850 hPa average summer meridional wind speed from June to August over (27°N~37°N, 110°E~120°E) encompassing the East Asian summer monsoon domain (Liu et al., 2014). The equation is as follows:

$$\mathrm{EASMI} = \overrightarrow{V_{850}}(27°\sim37°\mathrm{N},\ 110°\sim120°\mathrm{E})$$

The westerly wind index (WWI) is defined as the zonal difference of the 500 hPa averaged geopotential height over (35°N~50°N, 70°E~110°E) (Li et al., 2008). The equation is as follows:

$$\mathrm{WWI} = \overline{H_{35°}} - \overline{H_{50°}} = \frac{1}{17}\left[\sum_{\gamma=1}^{17} H(\gamma, 35°\mathrm{N}) - \sum_{\gamma=1}^{17} H(\gamma, 50°\mathrm{N})\right]$$

where H is the 500 hPa average height geopotential, γ is the number of longitudes taken along the latitude circle with a spacing of 2.5°.

https://doi.org/10.5194/cp-2023-71
Preprint. Discussion started: 15 September 2023

The East Asian winter monsoon index (EAWMI) is defined as the difference between the 300 hPa averaged zonal wind speed from December to February over (27.5°~37.5°N, 110°~170°E) and (50°~60°N, 80°~140°E) (Jhun and Lee, 2004). The equation is as follows:

$$\text{EAWMI} = \overrightarrow{U_{300}}(27.5°\sim37.5°\text{N}, 110°\sim170°\text{E}) - \overrightarrow{U_{300}}(50°\sim60°\text{N}, 80°\sim140°\text{E})$$

The calculation of EASMI, WWI, and EAWMI all rely on the NCEP Reanalysis 1 dataset.

2.4 Regional paleoclimatic proxy data

Here we compiled various paleoclimate records to reconstruct long-term climate variability and primarily paid close attention to paleo-precipitation and moisture changes since the LGM. We set three criteria to collect all the published proxy records from EA and CA in our study. Firstly, the records should be located primarily in the intersection encompassing the simultaneous region of rain and heat periods in EA and CA, which is in favor of investigating the difference and linkage in climate change modes from EA and CA. Accordingly, some typical records climatologically influenced by midlatitude westerlies in cores of EA and CA were selected for comparative analysis. Secondly, the proxies should be clearly indicative of changes in effective moisture or precipitation which have been confirmed by the original investigators. Third, the record length should cover the most period since LGM without documented depositional hiatuses. Fourth, the fluctuation and variation of proxy records should be predominantly forced by climate change, rather than human activities (Manoj et al., 2020; Chen et al.,

https://doi.org/10.5194/cp-2023-71
Preprint. Discussion started: 15 September 2023

2021c, 2022). Following the above criteria, a total of 42 proxy records from lakes, peats, loess, and stalagmites since the LGM were compiled for EA and CA (Fig. 1), enabling us to comprehensively review the LGM moisture evolution of the region. In light of seasonal signals of precipitation, 35 records are from the summer precipitation region, and seven records are from the winter precipitation region. Detailed information about these selected proxy records is presented in Table 1.

Table 1. Paleoclimate records selected in this study.

Code	Section name	Record type	Lat	Lon	Evaluation (m a.s.l)	Precipitation regime	Dating materials	Dating Method	Time period (cal ka BP)	Proxy	Proxy indication	References
1	Caspian Sea	Lake	41.93	50.67	-28	winter	Ostracods	^{14}C	12.4-2.4	Pollen	Moisture	Leroy et al. (2014)
2	YE section	Loess	37.60	55.43	383	winter	Quartz	OSL	11.8-0	$\delta^{13}C_{org}$	Moisture	Wang et al. (2020)
3	Ton Cave	Speleothem	38.40	67.34	3226	winter	Carbonate	U-Th	135-0	$\delta^{13}C$	Moisture	Cheng et al. (2016)
4	Valikhanov section	Loess	43.17	69.31	1000	winter	Bulk organic matter, charcoal	^{14}C	46-0	$\delta^{13}C$	Moisture	Ran and Feng (2014)
5	Osh section	Loess	40.61	73.01	1038	winter	Humin	^{14}C	30-0	Grain-size, MS	Effective moisture	Li et al. (2021)
6	Lake Karakul	Lake	39.02	73.53	3915	winter	plant remains, bulk sediments, living charophyte	^{14}C	~29-0	TIC, TOC, C/N, Grain-size, $\delta^{13}C_{carb}$, $\delta^{18}O$	Moisture	Heinecke et al. (2017)
7	BSK section	Loess	42.70	74.78	1432	winter	Bulk organic matter	^{14}C	26-0	Grain-size, MS, color proxies	Moisture	Li et al. (2020a)
8	Lake Issyk-Kul	Lake	42.50	77.10	1607	summer	Bulk sediments	^{14}C	12.75-3.6	$\delta^{18}O$, $\delta^{13}C$, Pollen, CaCO3, MS	Moisture	Ricketts et al. (2001); Leroy et al. (2021)
9	HC14 section	Loess	43.88	80.60	554	summer	Bulk organic matter	^{14}C	10-0	MS	Moisture	Jia et al. (2021)
10	ZS section	Loess	42.93	80.96	1650	summer	Quartz	OSL	12.6-0	Grain-size, MS	Moisture	Kang et al. (202

https://doi.org/10.5194/cp-2023-71
Preprint. Discussion started: 15 September 2023

												0)
11	Lake Sayram	Lake	41.50	81.03	2072	summer	Bulk sediments	^{14}C	13.8-0	Pollen	Moisture	Jiang et al. (2013, 2022)
12	Kesang Cave	Speleothem	42.87	81.75	~2000	summer	Carbonate	U-Th	22.8-0	$\delta^{18}O$	Precipitation	Cheng et al. (2012, 2016)
13	Yili section	Loess	43.86	81.97	928	summer	Charcoal	^{14}C	15-0	A/C ratio	Moisture	Li et al. (2011)
14	Lake Aibi	Lake	45.01	82.86	200	summer	Bulk sediments	^{14}C	13.8-0	Pollen	Moisture	Wang et al. (2013)
15	XEB section	Loess	43.42	82.99	888	summer	Quartz	OSL	12-0	Grain-size, MS	Moisture	Kang et al. (2020)
16	TLD16 section	Loess	43.36	83.02	1567	summer	Quartz	OSL	20-0	MS	Moisture	Jia et al. (2021)
17	ZKT section	Loess	43.53	83.30	846	summer	Bulk organic matter	^{14}C	16-0	MS	Moisture	Chen et al. (2016); Jia et al. (2021)
18	KS16 section	Loess	43.43	83.62	1314	summer	Quartz	OSL	12-0	MS	Moisture	Jia et al. (2021)
19	Baluk Cave	Speleothem	42.43	84.73	2400	summer	Carbonate	U-Th	9.3-0	Trace elements	Moisture	Liu et al. (2020)
20	LJW10 section	Loess	43.97	85.33	1462	summer	Quartz and K-feldspar	OSL	16-0	MS	Moisture	Chen et al. (2016)
21	Lake Bosten	Lake	41.94	86.76	1048	summer	Bulk organic matter, plant, tree leaves	^{14}C	8.2-0	Pollen	Moisture	Huang et al. (2009)
22	Narenxia peat	Peat	48.80	86.90	1760	summer	Bulk peat, lake mud	^{14}C	11.8-0	Pollen, $\delta^{13}C$	Annual precipitation	Feng et al. (2017); Zhang and Feng (2018)
23	Lake Kanas	Lake	48.70	87.01	1365	summer	Terrestrial plant macrofossils	^{14}C	13.4-0	Pollen	Annual precipitation	Huang et al. (2018)
24	Big Black peat	Peat	48.68	87.18	2168	summer	Cellulose	^{14}C	9.5-0	Pollen, $\delta^{18}O$, $\delta^{13}C$	Moisture	Xu et al. (201

https://doi.org/10.5194/cp-2023-71
Preprint. Discussion started: 15 September 2023

Climate of the Past Discussions
Open Access
EGU

												9)
25	Lake Wulungu	Lake	47.20	87.29	479	summer	Bulk organic matter	^{14}C	9.5-0	Pollen, $\delta^{13}C$, grain-size	Moisture	Liu et al. (2008)
26	ZL section	Loess	43.50	87.33	1756	summer	K-feldspar	OSL	10.8-0	MS	Moisture	Chen et al. (2016); Gao et al. (2019)
27	Tuolehaite peat	Peat	48.44	87.54	1700	summer	Plant residuals	^{14}C	10.6-0	Pollen	Moisture	Zhang et al. (2020)
28	Chaiwopu peat	Peat	43.35	88.30	800	summer	Plant, Bulk sediments	^{14}C	11.5-0	Pollen	Moisture	Yang et al. (2021)
29	Hoton Nurr	Lake	48.67	88.30	2083	summer	Bulk sediments	^{14}C	11.5-0	Pollen	Annual precipitation	Rudaya et al. (2009)
30	Lake Akkol	Lake	50.38	89.42	2204	summer	Bulk sediments	^{14}C	10-0	Pollen	Vegetation change	Blyakharchuk et al. (2007)
31	Achit Nuur	Lake	49.42	90.52	1444	summer	Bulk sediments, root, mollusk	^{14}C	22.6-0	$\delta^{18}O$	Annual precipitation	Sun et al. (2013)
32	Lake Lup-Nur	Lake	40.00	91.00	780	summer	Quartz	OSL	9-0	Soluble salt content, grain-size, pollen, ostracod	Moisture	Liu et al. (2016)
33	Lake Balikun	Lake	43.67	92.80	1575	summer	Bulk organic matter, plant macrofossils, pollen;	^{14}C	29.1-0	Pollen	Moisture	Tao et al. (2010); An et al. (2012); Zhao et al. (2015)
34	Bayan Nurr	Lake	49.98	93.95	932	summer	Bulk sediments	^{14}C	15-0	Pollen	Annual precipitation	Tian et al. (2014)
35	Qinghai Lake	Lake	37.00	100.00	3200	summer	Bulk organic matter	^{14}C	18-0	$\delta^{18}O$	summer monsoon precipitation	Shen et al. (2005); Liu et al. (2007)
36	Qilian section	Loess	38.16	100.27	2810	summer	Bulk organic matter	^{14}C	22-0	$\delta^{18}O$, $\delta^{13}C$	Effective moisture	Li et al. (2020b)
37	Lake Ulaan	Lake	44.53	103.63	1024	summer	Bull samples, quartz	^{14}C, OSL	17-0	TOC	Moisture	Lee et al. (2011, 201

https://doi.org/10.5194/cp-2023-71
Preprint. Discussion started: 15 September 2023

												3)
38	Dongge Cave	Speleothem	25.28	108.08	680	summer	Carbonate	U-Th	16-0	$\delta^{18}O$	summer monsoon precipitation	Dykoski et al. (2005)
39	Jiuxian Cave	Speleothem	33.5667	109.1	1495	summer	Carbonate	U-Th	19-0	$\delta^{18}O$	summer monsoon precipitation	Cai et al. (2010)
40	Lianhua Cave	Speleothem	29.483	109.533	455	summer	Carbonate	U-Th	12.5-0	$\delta^{18}O$	summer monsoon strength	Zhang et al. (2013)
41	Sanbao Cave	Speleothem	31.667	110.433	1900	summer	Carbonate	U-Th	13-0	$\delta^{18}O$	Summer rainfall	Dong et al. (2009)
42	Hulu Cave	Speleothem	32.50	119.17	90	summer	Carbonate	U-Th	Nov-75	$\delta^{18}O$	summer monsoon precipitation	Wang et al. (2001)

https://doi.org/10.5194/cp-2023-71
Preprint. Discussion started: 15 September 2023

Climate of the Past Discussions

2.5 Paleoclimatic simulations

The Paleoclimate Modeling Intercomparison Project (PMIP) was launched to coordinate and encourage the systematic study of General Circulation Models (GCMs) and to understand the mechanisms of climate change and the role of climate feedback (Joussaume et al., 1999) (Table 2). Eight coupled GCMs covering the LGM or MH from the PMIP3 database were selected to analyze the mechanisms of climate change in this study (Table 3), including bcc-csm1-1, CNRM-CM5, CCSM4, CSIRO-Mk3-6-0, GISS-E2-R, MIROC-ESM, FGOALS-s2, and MRI-CGCM3. The output data of the PMIP3 in the LGM and MH are available at htQTPs://esgf-node.llnl.gov/search/esgf-llnl/. By chiefly interpolating various climate variables on the common 1°×1° grid and then sorting the values of model simulations from minimum to maximum, we extracted the median value of all PMIP3 models used in this paper to evaluate the PMIP3 model simulations and acquire the scientific model simulation value.

Table 2. Boundary conditions and forcing for PMIP3-CMIP5 models at the LGM and MH.

Period	Eccentricity	Obliquity (°)	Longitude of perihelion (°)	CO_2 (ppm)	CH_4 (ppb)	N_2O (ppb)	Ice sheet	Vegetation
LGM	0.018994	22.949	114.425	185	350	200	Peltier (2004), 21 ka	Present day
MH	0.018682	24.105	0.87	280	650	270	Peltier (2004), 0 ka	Present day

Table 3. Basic information about climate models from PMIP3-CMIP5 used in this study.

Model	Institute	Resolutions	Variables*	References
bcc-csm1-1	Beijing Climate Center, China Meteorological Administration, China	64×128 (17)	ua, va, zg, hus, psl, pr, tas	Randall et al. (2007)
CNRM-CM5	Centre National de Recherches Météorologiques, France	128×256 (17)	ua, va, zg, hus, psl, pr, tas	Voldoire et al. (2013)

https://doi.org/10.5194/cp-2023-71
Preprint. Discussion started: 15 September 2023

Climate of the Past Discussions
Open Access

CCSM4	National Center for Atmospheric Research, USA	288×192 (17)	ua, va, zg, hus, psl, pr, tas	Gent et al. (2011)
CSIRO-Mk3-6-0	Australian Commonwealth Scientific and Industrial Research Organization Marine and Atmospheric Research in collaboration with the Queensland Climate Change Centre of Excellence, Australia	96×192 (18)	ua, va, zg, hus, psl, pr, tas	Rotstayn et al. (2010)
GISS-E2-R	NASA Goddard Institute for Space Studies, USA	144×90 (17)	ua, va, zg, hus, psl, pr, tas	Schmidt et al. (2014)
MIROC-ESM	Japan Agency for Marine-Earth Science and Technology, Japan	128×64 (35)	ua, va, zg, hus, psl, pr, tas	Watanabe et al. (2011)
FGOALS-s2	LASG-CEES. China	108×128 (17)	ua, va, zg, hus, psl, pr, tas	Briegleb et a1. (2004)
MRI-CGCM3	Meteorological Research Institute, Japan	320×160 (23)	ua, va, zg, hus, psl, pr, tas	Yukimoto et al. (2012)

*: ua means eastward_wind; va means northward wind; zg geopotential Height; hus near-surface relative humidity; psl means sea surface pressure; pr means precipitation; tas means near-surface temperature

3. Results

3.1 Seasonal signals at short-term timescales

To obtain the spatial distribution characteristics of the precipitation anomalies in EA and CA under the context of seasonal signals, we conducted an EOF analysis on the precipitation standardized anomaly field over 1971-2020. Figure 2a-d shows the spatial distribution and time series of EOF decomposition of mean annual precipitation. The variance contribution rate of the first mode is 10.29%, showing an obvious dipole mode. The center of negative values is in the core region of CA mainly belonging to the winter precipitation regime, while the positive values are in the south and north of EA located in summer precipitation regions (Fig. 2a). This opposite distribution indicates that the mean annual precipitation in EA and CA have a see-saw pattern. Additionally, the first

https://doi.org/10.5194/cp-2023-71
Preprint. Discussion started: 15 September 2023

mode exhibits interdecadal and interannual changes according to the PC1 (Fig. 2b). The variance contribution rate of the second mode is 8.79%, indicating zonal dipole distribution characteristics (Fig. 2c). The center of positive values is in the north of EA, and the center of negative values is in the north of CA, also displaying the spatial diversity of mean annual precipitation in EA and CA (Fig. 2c).

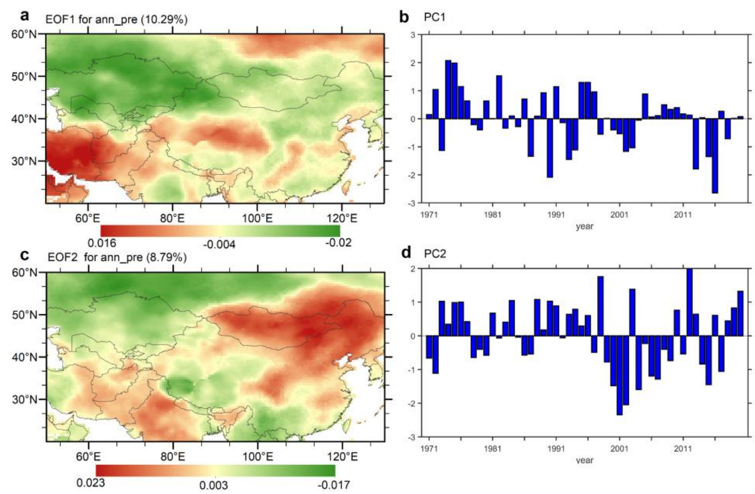

Figure. 2 The EOF modes and corresponding time series of annual mean precipitation in EA and CA over 1971-2020.

In order to further explore the contribution of seasonal signals of precipitation to dry/wet status in EA and CA, we conducted the EOF analysis on the seasonal precipitation in spring, summer, autumn, and winter. The variance contribution rate of the first mode in precipitation of four seasons is shown in Fig. 3. The first mode of spring and autumn precipitation does not show obvious distribution characteristics, and the contribution rate is relatively uniform, indicating that spring and autumn precipitation have no special precipitation contribution to EA and CA (Fig. a and c). In summer precipitation, the centers of positive values are mainly distributed in the north of EA, while the negative values are mainly distributed in CA and south of EA (Fig.

https://doi.org/10.5194/cp-2023-71
Preprint. Discussion started: 15 September 2023

3b). This spatial distribution indicates that summer precipitation mainly affects the dry/wet status in northern EA and the east of CA belonging to the simultaneous region of rain and heat periods, which is in contrast to the core region of CA. In winter precipitation, the center of the positive value is located in the CA and north of EA, showing the significant contribution of winter precipitation to CA (Fig. 3d). It is worth noting that a certain degree of similarities exists in both summer and winter precipitation of EA and CA, indicating the impact of seasonal precipitation on the linkage of dry/wet status in EA and CA at short-term timescales.

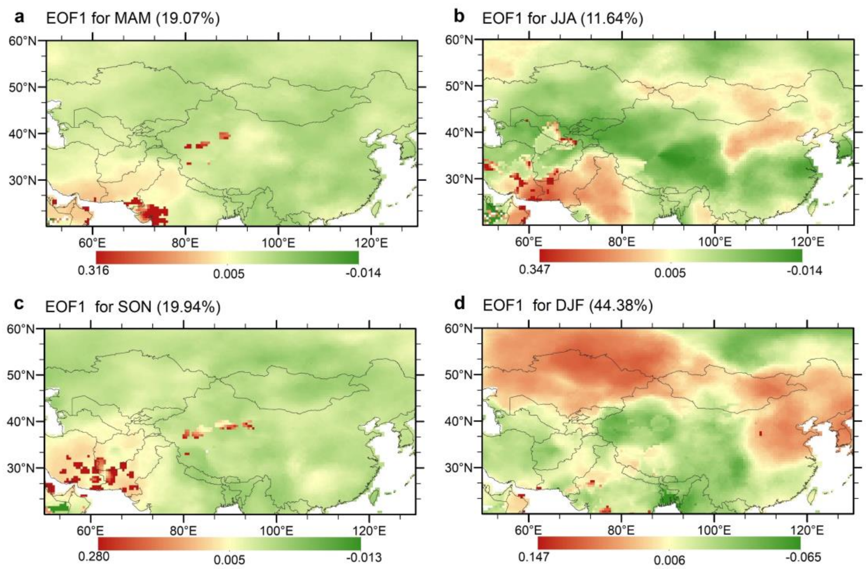

Figure. 3 The first EOF modes of precipitation in spring (March, April, and May, MAM) (a), summer (June, July, and August, JJA) (b), autumn (September, October, and November, SON) (c), and winter (December, January, and February, DJF) (d) in EA and CA over 1971-2020.

Existing studies emphasized the role of water vapor sources in affecting interannual to interdecadal variability of precipitation (Chen and Huang, 2012; Huang et al., 2015a; Peng and Zhou, 2017; Wei et al., 2017). Therefore, by analyzing the EOF results of water vapor content in the whole layer, this study investigates the general characteristics

https://doi.org/10.5194/cp-2023-71
Preprint. Discussion started: 15 September 2023

of the spatial distribution of water vapor in EA and CA and discusses the influence mechanism of seasonal signals on dry/wet status in EA and CA at short-term timescales. The EOF1 of the mean annual water vapor shows that the core region of CA is dominated by positive values, while EA and eastern CA are synchronized with negative values (Fig. 4a). The same spatial distribution mode is also reflected in the EOF1 of water vapor difference between summer and winter half-year. To summarize, the water vapor in EA and CA shows a dipole out-of-phase pattern between the simultaneous region of rain and heat periods and the non-simultaneous region of rain and heat periods (Fig. 4b). This implies that the content and source of water vapor are the important reason why the dry/wet status in eastern CA is linked to that in EA by seasonal signals of precipitation.

Climate of the Past
Discussions
Open Access

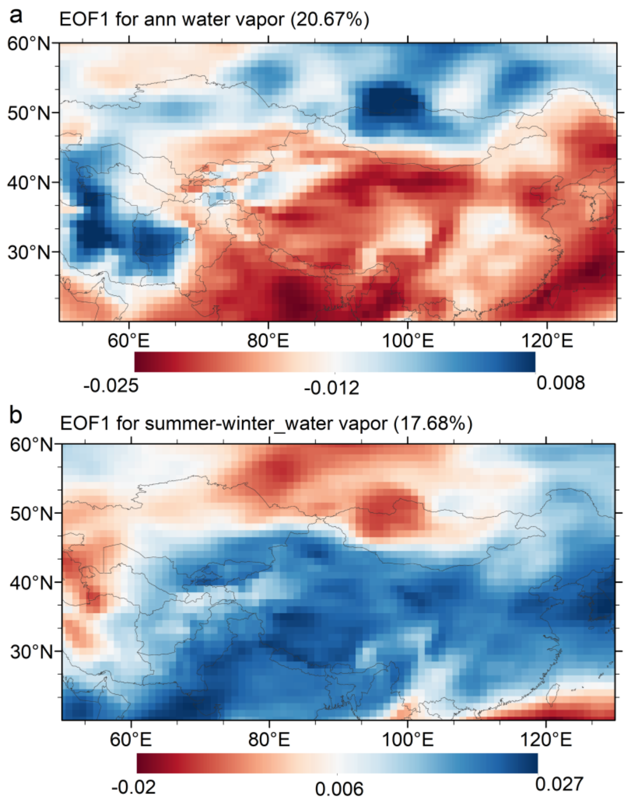

Figure. 4 a, the EOF1 modes of annual mean integral water vapor in EA and CA over 1979-2018; b, the EOF1 modes of integral water vapor difference between summer and winter in EA and CA over 1979-2018.

3.2 Spatiotemporal variation of dry/wet status and seasonal signals at long-term timescales

In the last decade, many paleoclimate records with a relatively high resolution, reliable chronology, and unambiguous proxies have been published to discuss the long-term timescale climate evolution in EA and CA. Forty-two moisture records from individual sites are used to illustrate the spatiotemporal pattern of dry/wet status since the LGM in EA and CA (Fig. 7). During the LGM, most regions in EA and CA are in moderately dry condition (Fig. 7a). However, moderately wet and wet conditions partly exist in the east of CA. According to the model simulation, Yu et al. (2000) concluded

https://doi.org/10.5194/cp-2023-71
Preprint. Discussion started: 15 September 2023

that the low temperature in the cold period causes decreasing evaporation, with the enhanced westerlies driven by expanding land ice sheets, forming the high lake level in western China and the low lake level in eastern China during the LGM. During the early Holocene (EH), CA is dominated by a dry climate, while EA is moderately wet. At the same time, there were many records in the east of CA similar to the dry/wet status of EA. During the MH, the dry/wet status is mainly wet in the core region of CA and gradually turns into moderately wet and even dry conditions in the east of CA, while the EA remains moderately wet. By the late Holocene (LH), the EA is characterized by dry status, while CA is wet. In particular, the dry condition during the LGM and the wet climate during the EH and MH also reflect another meaning of seasonal signals derived from the simultaneity of rain and heat periods at long-term timescales, namely the "dry-cold" pattern and "wet-warm" pattern.

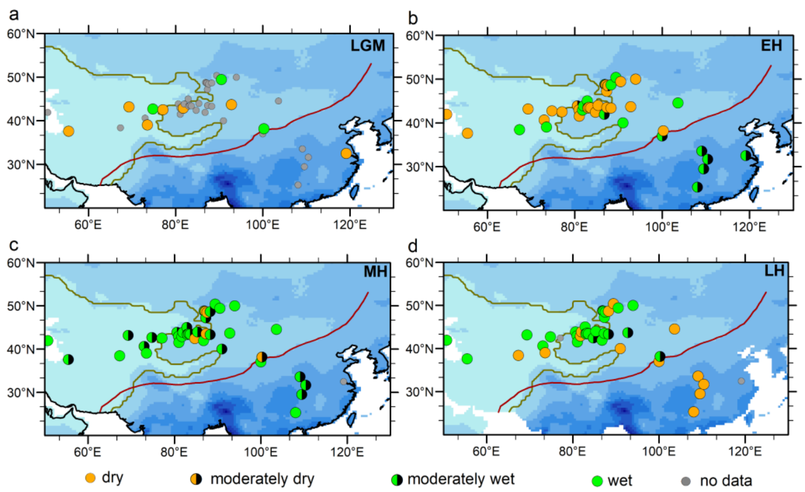

Figure. 7 Spatio-temporal characteristics of the dry/wet status from 42 records since the LGM, based on the confirmation of original investigators during the LGM, early Holocene (EH), mid Holocene (MH), and late Holocene (LH). Records with an incomplete stage are shown by a gray dot. Four summarized levels of dry/wet status: wet, moderately wet, moderately dry, and dry.

In detail, we further performed a comparative analysis of time series of typically

https://doi.org/10.5194/cp-2023-71
Preprint. Discussion started: 15 September 2023

proxy record in EA and CA (Fig. 8). The reconstructed precipitation covering the past 22,600 years from Achit Nuur suggests the wet periods from 22,600 to 13,200 cal BP (Fig. 8c). Pollen record from the Caspian Sea, controlled by the westerlies, displays that the terrestrial vegetation around the Caspian Sea changed from desert/desert steppe during the last glacial to dry shrubland/forest during the Holocene, revealing the continuous wetting process since the EH and the wettest LH (Fig. 8a). Meanwhile, results of climatically-sensitive magnetic properties from the Xinjiang loess demonstrate that the relatively wet conditions are generally formed after ~6,000 cal BP, with the wettest climate occurring during the LH (Fig. 8b). However, there is still partially contradictory for dry/wet changes on long-term timescales in CA, which are different from CA but similar to EA. Herzschuh. (2006) comprehensively analyzed 75 paleoclimatic records in CA and revealed that wet conditions occurred during the EH and MH, while the LGM was characterized by the dry climate (Fig. 8h), indicating the similarity with the monsoon climate represented by the speleothem $\delta^{18}O$ records from Dongge Cave and Hulu Cave (Fig. 8d). High precipitation in the EH and MH, indicated by $\delta^{18}O$ records of ostracod shells from Qinghai Lake, shows that the climate in Qinghai Lake since the late glacial reflects the monsoon-dominated characteristic (Fig. 8e). The climate in Ulaan Nuur is wettest during the EH, humid during the MH and dry in the LH, embodying a typical characteristic of the East Asian summer monsoon (Fig. 8f). Based on the sediment cores from Lake Karakul and Lake Issyk-Kul, the EH and MH is characterized by wetter conditions in the region, and the lake level remained low during the LGM (Fig. 8g and j). Furthermore, the regional climate in western China,

https://doi.org/10.5194/cp-2023-71
Preprint. Discussion started: 15 September 2023

Climate of the Past Discussions

inferred from the speleothem oxygen-carbon isotope in Kesang Cave, suggests a close coupling with the Asian summer monsoon (Fig. 8i). The lake level and climate reconstructed results also conducted that the "dry-cold" pattern triggered a substantial lowering of lake level in most of arid western China, challenging the traditional view of "wet-cold" pattern and high lake levels during the LGM (Zhao et al., 2015).

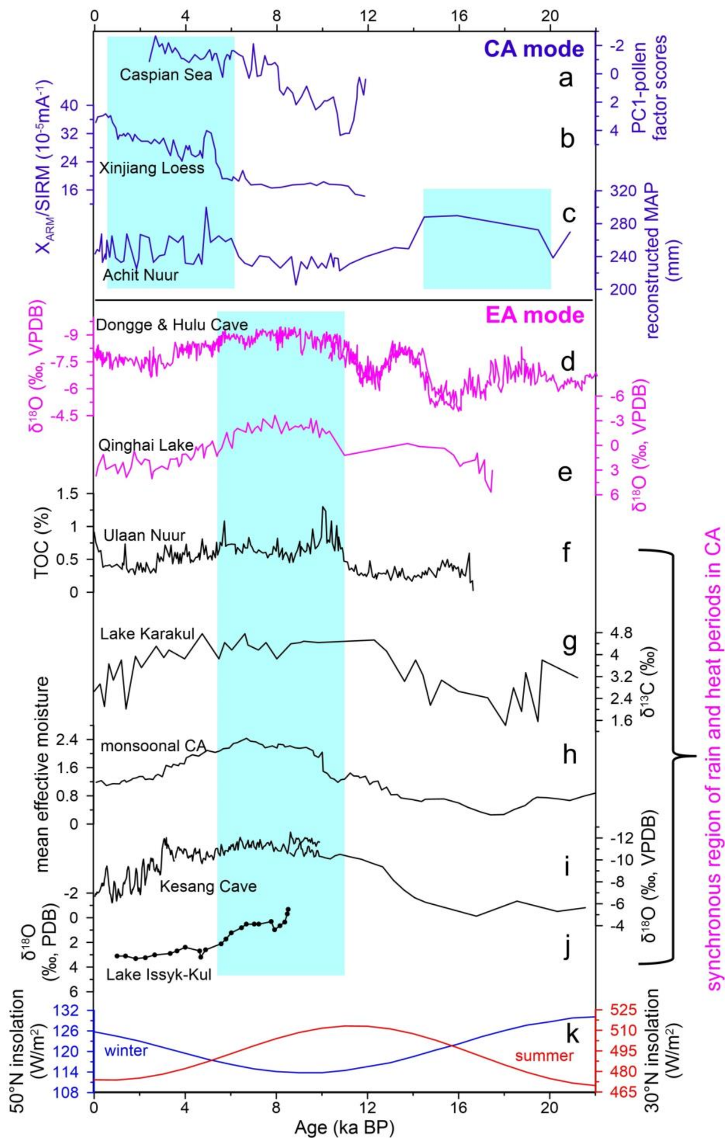

https://doi.org/10.5194/cp-2023-71
Preprint. Discussion started: 15 September 2023

Figure. 8 A comparison of proxy variability recorded in EA and CA. a Pollen record from the Caspian Sea (Leroy et al., 2014); b X_{ARM}/SIRM in the LJW10 section of the Xinjiang Loess (Chen et al., 2016); c Reconstructed MAP (mean annual precipitation) from Achit Nuur (Sun et al., 2013); d speleothem $\delta^{18}O$ values records from Dongge Cave and Hulu Cave (Yuan et al., 2004; Wang et al., 2001); e $\delta^{18}O$ of ostracode shells from Qinghai Lake (Liu et al., 2007); f TOC (Total organic carbon) from Ulaan Nuur (Lee et al., 2013); g $\delta^{13}C$ from Lake Karakul (Heinecke et al., 2017; Mischke et al., 2017); h Mean effective moisture from monsoonal Central Asia (Herzschuh, 2006); i $\delta^{18}O$ from Kesang Cave (Cheng et al., 2016); j $\delta^{18}O$ from Lake Issyk-Kul (Ricketts et al., 2001); k Summer (red line) insolation at 30°N and winter (blue line) insolation at 50°N (Berger, 1978);. Blue shadows indicate the wet period of paleoclimate proxies.

4. Discussion

4.1 Possible dynamics of seasonal signals at short-term timescales

EOF analysis of precipitation and water vapor consistently verifies that the connection between EA and the east of CA exists under the traditional differentiation between EA and the core region of CA. Considering that the east of CA is present as the summer precipitation regime. Therefore, we propose that seasonal signals of precipitation contribute to the connection between EA and the east of CA.

https://doi.org/10.5194/cp-2023-71
Preprint. Discussion started: 15 September 2023

Climate of the Past
Discussions
Open Access

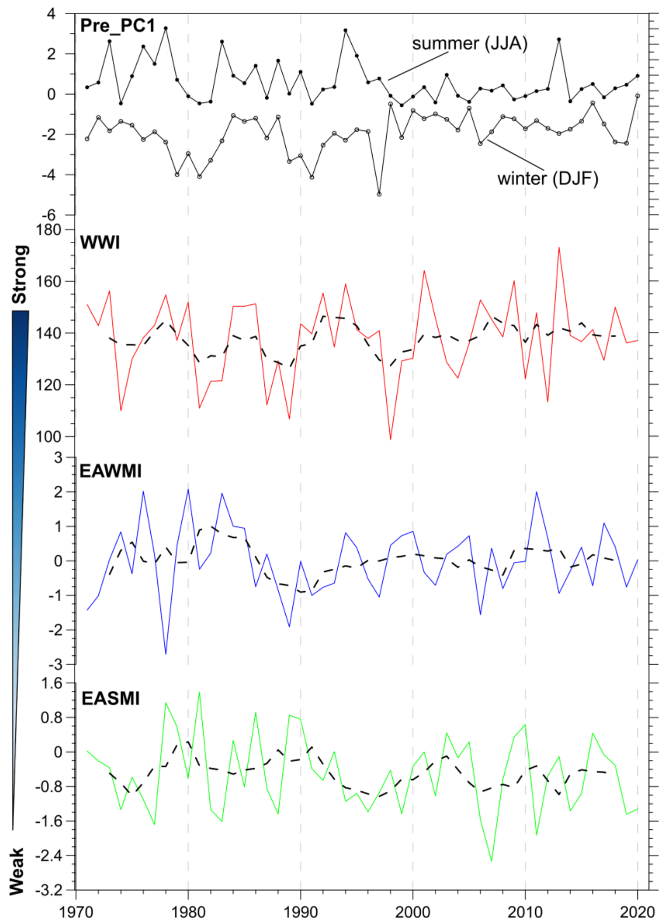

Figure. 5 The time series of the precipitation PC1 in summer, winter, WWI, EAWMI, and EASMI over 1971-2020.

Generally, atmosphere circulations have important effects on the spatial distribution and the transportation of water vapor. In order to explore the influence of the modern air-sea circulation system on the summer and winter precipitation, we analyzed the time series of the precipitation PC1, WWI, EAWMI, EASMI, NAO, PDO, and ENSO over 1971 to 2020 (Fig. 5 and 6). Comparing the winter precipitation PC1 with WWI and EAWMI (Fig. 5), the weakening of the westerlies and winter monsoons is usually accompanied by an increase in winter precipitation. However, there is not a

https://doi.org/10.5194/cp-2023-71
Preprint. Discussion started: 15 September 2023

significant relationship between PC1 of summer precipitation and EASMI. As shown in Figure. 6, summer PDO and ENSO are basically similar to winter PDO and ENSO. However, the markable discrepancy exists in the evolution of winter NAO and summer NAO. The NAO and ENSO index presents interannual timescale variation, and the PDO index has an interdecadal timescale cycle. The NAO index and the winter precipitation PC1 have a positive correlation, suggesting that the North Atlantic may have certain effects on the winter precipitation through the air-sea interaction. Positive values of the NAO index are usually accompanied by stronger midlatitude westerlies and increased water vapor content from the North Atlantic. The PDO and ENSO, however, were related to the summer precipitation PC1. The development of winter precipitation at interdecadal timescales was not connected with PDO, whereas there is a positive correlation before the 2000s between summer precipitation and PDO.

https://doi.org/10.5194/cp-2023-71
Preprint. Discussion started: 15 September 2023

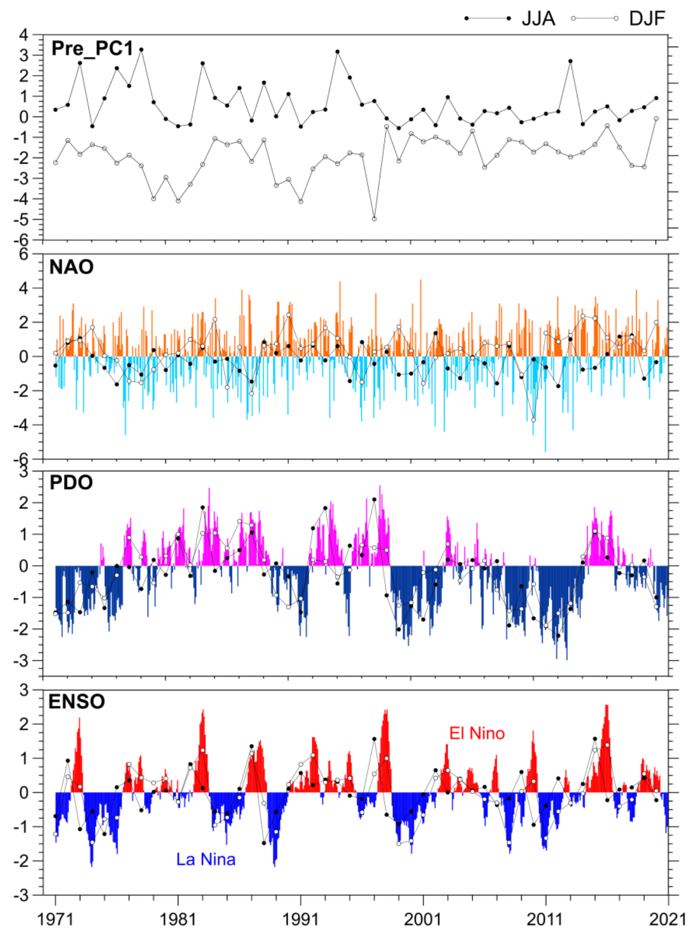

Figure. 6 The time series of the precipitation PC1 in summer, winter, and annual mean, NAO, PDO, and ENSO over 1971-2020.

A majority of relevant studies stand for that precipitation variations in CA are subjected to water vapor transported by the mid-latitude westerlies, where the monsoonal water vapor source is hard to reach (Huang et al., 2015a; Guan et al., 2019). Abundant moisture is brought to CA from polar airmass, North Atlantic and the eastern Mediterranean Sea, and continues to diffuse eastward to the arid region of northwest China (Lioubimtseva, 2014). Meanwhile, several studies in recent years found that the anti-phase pattern between the East Asian summer monsoon and the westerlies causes

https://doi.org/10.5194/cp-2023-71
Preprint. Discussion started: 15 September 2023

the seesaw phenomenon of precipitation variation in northwest China (the east of CA in this study) (Zhang et al., 2019; Wu et al., 2019). However, Chen et al. (2021a) proposed that the East Asian summer monsoon plays an important role in the interdecadal variability of summer precipitation in CA through the transportation of summer water vapor from the Indian and Pacific Oceans to eastern CA. Additionally, Huang et al. (2015b) stated that increased summer precipitation in the Tarim Basin is mainly related to the weakened Indian summer monsoon. In addition, the large-scale topography, such as the Qinghai-Tibet Plateau, causes the westerlies to flow around the plateau rather than over it, which in turn influences the local transport of water vapor and results in local precipitation changes (Xie et al., 2014). Therefore, the atmospheric circulation and topographic factors bear on the transportation and content of water vapor at short-term timescales, which makes the east of CA with summer precipitation regime different from the core region of CA, but linked to the EA.

4.2 Possible dynamics of seasonal signals at long-term timescales

Studying the mechanism of paleoclimate change in EA and CA during the LGM and MH, with model simulation, is of great significance for assessing future hydroclimate changes. The results of paleoclimate simulations explain the difference and linkage in the dry/wet status from EA and CA under the framework of seasonal signals at long-term timescales. During the LGM, lower summer insolation increases the meridional temperature difference and sea level pressure in the summer largely (Fig. 8k; 9a and c), leading to the strengthening of the westerlies (Fig. 10a) and further

https://doi.org/10.5194/cp-2023-71
Preprint. Discussion started: 15 September 2023

increasing precipitation in the core region of CA (Fig. 9e). Given the weakening of the LGM summer monsoon and the complex control factors (Fig. 10c), however, the summer precipitation in the east of CA is weaker than that of MH (Fig. 9e), which is consistent with the dry/wet status in EA and reflects the linkage between EA and the east of CA caused by the summer precipitation regime. Although the westerlies weaken in the LGM winter (Fig. 10b), the higher winter insolation contributes to the general warming in CA and EA (Fig. 8k; 9b), resulting in lower relative humidity (Fig. 9d). According to climatological theory (Barry and Richard, 2009), the decrease in relative humidity means the increase in saturated water vapor pressure, which ultimately leads to the increasing precipitation (Fig. 9f). Therefore, this elaborates the asynchrony of the long-term dry/wet status in EA and CA under the control of seasonal signals.

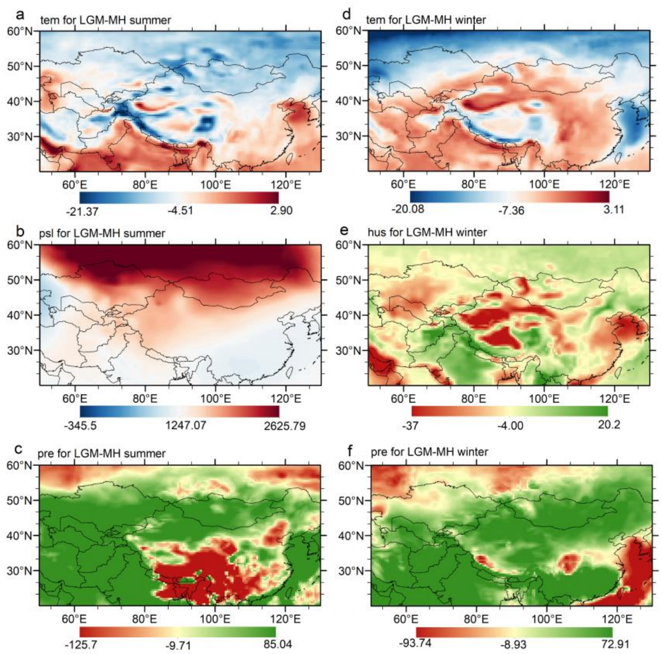

Figure. 9 Summer differences of temperature (tem) (a), sea level pressure (psl) (c), precipitation (pre) (e), 700 hPa wind field (g), and 200 hPa wind field (h) for LGM-MH; and winter differences of temperature (b), relatively humid

https://doi.org/10.5194/cp-2023-71
Preprint. Discussion started: 15 September 2023

(hus) (d), precipitation (f), and 200 hPa wind field (i) for LGM-MH in EA and CA based on the PMIP3-CMIP5 multi-model ensemble.

Investigating the past climate is key to informing future climate change (Tierney et al., 2020). From the perspective of paleoclimatology, monsoon and westerlies vary greatly between LGM and MH, modulated by primary forces such as orbital insolation, greenhouse gas, and ice sheets (Oster et al., 2015; Bereiter et al., 2015; Sime et al., 2016). Paleoclimate records clearly indicate the wet status during the LGM and LH in CA and the MH wet in EA (Fig. 8). Specifically, the dry/wet status in CA, affected by the westerlies and characterized by wet climate conditions during the LGM and mid- and late-Holocene, is opposite to that in monsoon-dominated EA. However, the proxy records in CA similar to the monsoon evolution are located in the modern summer precipitation region. From the perspective of precipitation seasonality, there are two different precipitation regimes within CA. The core region of CA has a Mediterranean climate (winter precipitation regime), with a dry summer and with seasonal precipitation from early winter to late spring (Fig. 1); whereas, in the east of CA, including northwest of China and west and south of Mongolia, the summer precipitation contributes more (summer precipitation regime; Fig. 1). Therefore, summer precipitation regime may be a potential forcing factor for the linkage of paleoclimate reconstruction between EA and the east of CA, and the difference in precipitation regime may result in a divergent moisture history in EA and the core region of CA.

https://doi.org/10.5194/cp-2023-71
Preprint. Discussion started: 15 September 2023

Climate of the Past
Discussions
Open Access

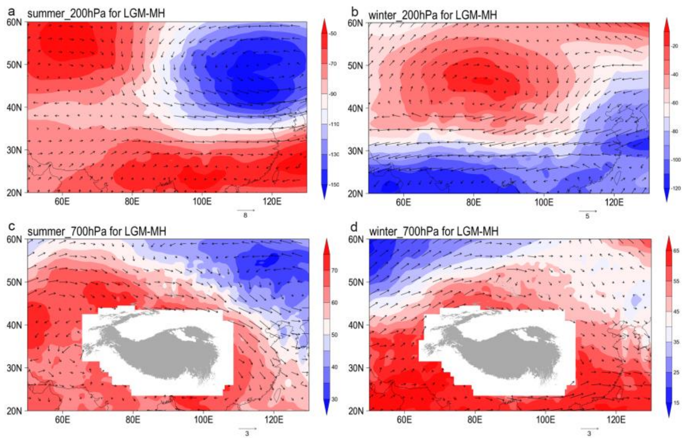

Figure. 10 Summer differences of 200 hPa wind field (a) and 700 hPa wind field (c) for LGM-MH; and winter differences of 200 hPa wind field (b) and 700 hPa wind field (d) for LGM-MH in EA and CA based on the PMIP3-CMIP5 multi-model ensemble.

As a whole, our results provide a hypothesis that seasonal signals of precipitation derived from the simultaneity of rain and heat periods govern the difference and linkage in dry/wet status from EA and CA at multi-time scales. With recent global warming, some recent work also points out increasing summer precipitation in arid CA (Chen et al., 2021a; Ren et al., 2022). Meanwhile, the phenomenon of warmer and wetter climates coincides with the simultaneity of rain and heat periods (Hu and Han, 2022). Future work should focus on the fusion of multiple datasets and high-precision climate simulation designed to evaluate the mechanism.

5. Conclusion

The summer precipitation regime in EA and the east of CA and the winter precipitation regime in the core region of CA reveal seasonal signals of precipitation. Using the EOF method, this study analyzes the spatiotemporal variations of precipitation in EA and CA. Results reveal that seasonal signals derived from the

https://doi.org/10.5194/cp-2023-71
Preprint. Discussion started: 15 September 2023

Climate of the Past
Discussions

simultaneity of rain and heat periods are important factors linking climate change modes in EA and CA at short-term timescales. A compilation of 42 proxy records with reliable chronologies enables us to reassess the dry/wet status in EA and CA since the LGM. Concurrently, paleoclimate records reflect seasonal signals triggered by the insolation at long-term timescales. The multi-model simulations of multiple climatic elements explain the climate mechanism of differences and linkage in dry/wet status from EA and CA. In the traditional context of asynchronous dry/wet status between summer precipitation regions and winter precipitation regions, we believe that regional linkages also exist in EA and CA affected by seasonal signals.

Acknowledgment

This research was supported by the National Natural Science Foundation of China (Grant No. 42077415); the Second Tibetan Plateau Scientific Expedition and Research Program (STEP) (Grant No. 2019QZKK0202); the Strategic Priority Research Program of Chinese Academy of Sciences (Grant No. XDA20100102); the 111 Project (BP0618001).

References

An, C.B., Feng, Z.D., Barton, L., 2006. Dry or humid? Mid-Holocene humidity changes in arid and semi-arid China. Quat. Sci. Rev. 25, 351-61.

An, C.B., Lu, Y.B., Zhao, J.J., Tao, S.C., Dong, W.M., Li, H., Jin, M., Wang, Z.L., 2012. A high-resolution record of Holocene environmental and climatic changes from Lake Balikun (Xinjiang, China): implications for central Asia. Holocene 22, 43-52.

Barichivich, J., Osborn, T.J., Harris, I., van der Schrier, G., Jones, P.D., 2021. Monitoring global drought using the self-calibrating Palmer Drought Severity Index [in \State of the Climate in 2020\]. Bulletin of the American Meteorological

https://doi.org/10.5194/cp-2023-71
Preprint. Discussion started: 15 September 2023

Society 101. S51-S52.

Barry, R.G., Richard, J.C., 2009. Atmosphere, weather and climate. Routledge.

Bereiter, B., Eggleston, S., Schmitt, J., Nehrbass - Ahles, C., Stocker, T. F., Fischer, H., Kipfstuhl, S., Chappellaz, J., 2015. Revision of the EPICA Dome C CO2 record from 800 to 600 kyr before present. Geophys. Res. Lett. 42, 542-549.

Blyakharchuk, T.A., Wright, H.E., Borodavko, P.S., van der Knaap, W.O., Ammann, B., 2007. Late glacial and Holocene vegetational history of the Altai mountains (southwestern tuva republic, siberia). Palaeogeogr. Palaeoclimatol. Palaeoecol. 245, 518-534.

Briegleb, B.P., Bitz, C.M., Hunke, E.C., Lioscomb, W.H., Holland, M.M., Schramm, J.L., Moritz, A.R., 2004. Scientific description of the sea ice component in the community climate system model. Version, 3, 70.

Cai, Y., Tan, L., Cheng, H., An, Z., Edwards, R. L., Kelly, M. M., Kong, X., Wang, X., 2010. The variation of summer monsoon precipitation in central China since the last deglaciation. Earth Planet Sci. Lett. 291, 21-31.

Chen, C., Zhang, X., Lu, H., Jin, L., Du, Y., Chen, F., 2021a. Increasing summer precipitation in arid central Asia linked to the weakening of the East Asian summer monsoon in the recent decades. Int. J. Climatol. 41, 1024-1038.

Chen, F., Chen, J., Huang, W., 2021b. Weakened East Asian summer monsoon triggers increased precipitation in Northwest China. Sci. China Earth Sci. 64, 835-837.

Chen, F., Chen, J., Huang, W., Chen, S., Huang, X., Jin, L., Jia, J., Zhang, X., An, C., Zhang, J., Zhao, Y., 2019. Westerlies Asia and monsoonal Asia: spatiotemporal differences in climate change and possible mechanisms on decadal to suborbital timescales. Earth Sci. Rev. 192, 337-354.

Chen, F., Jia, J., Chen, J., Li, G., Zhang, X., Xie, H., Xia, D., Huang, W., An, C., 2016. A persistent Holocene wetting trend in arid central Asia, with wettest conditions in the late Holocene, revealed by multi-proxy analyses of loess-paleosol sequences in Xinjiang, China. Quat. Sci. Rev. 146, 134-146.

Chen, F., Chen, J., Huang, W., 2009. A discussion on the westerly-dominated climate model in mid-latitude Asia during the modern interglacial period. Earth Sci. Front. 16, 23-32 (in Chinese with English abstract).

Chen, F., Yu, Z., Yang, M., Ito, E., Wang, S., David, B.M., Huang, X., Zhao, Y., Sato, T., Birks, H.J.B., Boomer, I., Chen, J., An, C., Wünnemann, B., 2008. Holocene moisture evolution in arid Central Asia and its out-of-phase relationship with Asian monsoon history. Quat. Sci. Rev. 27, 351-364.

Chen, G., Huang, R., 2012. Excitation mechanisms of the tele-connection patterns affecting the July precipitation in North-west China. J. Clim. 25, 7834-7851.

Chen, S., Chen, J., Lv, F., Liu, X., Huang, W., Wang, T., Liu, J., Hou, J., Chen, F., 2022. Holocene moisture variations in arid central Asia: Reassessment and reconciliation. Quat. Sci. Rev. 297, 107821.

Chen, S., Liu, J., Wang, X., Zhao, S., Chen, J., Qiang, M., Liu, B., Xu, Q., Xia, D., Chen, F., 2021c. Holocene dust storm variations over northern China: transition from a natural forcing to an anthropogenic forcing. Sci. Bull. 66, 2516-2527.

Cheng, H., Sp€otl, C., Breitenbach, S.F.M., Sinha, A., Wassenburg, J.A., Jochum, K.P.,

https://doi.org/10.5194/cp-2023-71
Preprint. Discussion started: 15 September 2023

Scholz, D., Li, X.L., Peng, Y.B., Lv, Y.B., Zhang, P.Z., Votintseva, A., Loginov, V., Ning, Y.F., Kathayat, G., Edwards, R.L., 2016. Climate variations of Central Asia on orbital to millennial timescales. Sci. Rep. 6, 36975.

Cheng, H., Zhang, P., Sp€otl, C., Edwards, R.L., Cai, Y., Zhang, D., Sang, W., Tan, M., An, Z., 2012. The climatic cyclicity in semiarid-arid central Asia over the past 500,000 years. Geophys. Res. Lett. 39, L01705.

Dykoski, C.A., Edwards, R.L., Cheng, H., Yuan, D., Cai, Y., Zhang, M., Lin, Y., Qing, J., An, Z., Revenaugh, J., 2005. A high-resolution, absolute-dated Holocene and deglacial Asian monsoon record from Dongge Cave, China. Earth Planet. Sci. Lett. 233, 71-86.

Feng, Z.D., Sun, A.Z., Abdusalih, N., Ran, M., Kurban, A., Lan, B., Zhang, D.L., Yang, Y.P., 2017. Vegetation changes and associated climatic changes in the southern Altai Mountains within China during the Holocene. Holocene 27, 683-693.

Gao, F.Y., Jia, J., Xia, D.S., Lu, C.C., Lu, H., Wang, Y.J., Liu, H., Ma, Y.P., Li, K.M., 2019. Asynchronous Holocene climate optimum across mid-latitude Asia. Palaeogeogr. Palaeoclimatol. Palaeoecol. 518, 206e214.

Gent, P.R., Danabasoglu, G., Donner, L.J., Holland, M.M., Hunke, E.C., Jayne, S.R., Lawrence, D.M., Neale, R.B., Rasch, P.J., Vertenstein, M., 2011. The community climate system model version 4. J. Clim. 24, 4973-4991.

Guan, X., Yang, L., Zhang, Y., & Li, J. (2019). Spatial distribution, temporal variation, and transport characteristics of atmospheric water vapor over Central Asia and the arid region of China. Global Planet. Change 172, 159-178.

Han, S.T., Wu, N.Q., Li, Z.Z., 1993. Inland climate changes in Dzungaria during the late Pleistocene Epoch. Geographical Research. 12, 47-54 (in Chinese with English abstract).

Han, S.T., Qu, Z., 1992. Inland Holocene climatic features recorded in Balikun lake, northern Xinjiang. Science in China Series B-Chemistry, Life Sciences & Earth Sciences (in Chinese) 11, 1201-1209.

Harris, I., Jones, P.D., Osborn, T.J., Lister, D.H., 2014. Updated high-resolution grids of monthly climatic observations-the CRU TS3.10 Dataset. Int. J. Climatol. 34, 623-642.

Heinecke, L., Mischke, S., Adler, K., Barth, A., Biskaborn, B.K., Plessen, B., Ingmar, N., Gerhard, K., Ilhomjon, R., Herzschuh, U., 2017. Climatic and limnological changes at Lake Karakul (Tajikistan) during the last ~29 cal ka. J. Paleolimnol. 58, 317-334.

Hersbach, H., Bell, B., Berrisford, P., Hirahara, S., Horányi, A., Muñoz-Sabater, J., Nicolas, J., Peubey, C., Radu, R., Schepers, D., Simmons, A., Soci, C., Abdalla, S., Abellan, X., Balsamo, G., Bechtold, P., Biavati, G., Bidlot, J., Bonavita, M., . . . Hersbach, H., 2020. The ERA5 global reanalysis. Quarterly Journal of the Royal Meteorological Society, 146, 1999-2049.

Herzschuh, U., 2006. Palaeo-moisture evolution in monsoonal central Asia during the last 50,000 years. Quat. Sci. Rev. 25, 163-178.

Hu, Q., Han, Z.H., 2022. Northward Expansion of Desert Climate in Central Asia in Recent Decades. Geophys. Res. Lett. 49, e2022GL098895.

Huang, W., Chen, J.H., Zhang, X.J., Feng, S., Chen, F.H., 2015a. Definition of the core zone of the "westerlies-dominated climatic regime", and its controlling factors during the instrumental period. Sci. China Earth Sci. 58, 676-684.

Huang, W., Feng, S., Chen, J. and Chen, F. 2015b. Physical mechanisms of summer precipitation variations in the Tarim basin in northwestern China. J. Clim. 28, 3579-3591.

Huang, X.Z., Chen, F.H., Fan, Y.X., Yang, M.L., 2009. Dry late-glacial and early Holocene climate in arid central Asia indicated by lithological and palynological evidence from Bosten Lake, China. Quat. Int. 194, 19-27.

Hurrell, J.W., Deser, C., 2009. North Atlantic climate variability: The role of the North Atlantic Oscillation. J. Mar. Syst., 78, 28-41.

Hurrell, J.W., 1995. Decadal Trends in the North Atlantic Oscillation: Regional Temperatures and Precipitation. Science 269, 676-679.

Jia, J., Chen, J.H., Wang, Z.Y., Chen, S.Q., Wang, Q., Wang, L.B., Yang, L.W., Xia, D.S., Chen, F.H., 2021. No evidence for an anti-phased Holocene moisture regime in mountains and basins in Central Asian: records from Ili loess, Xinjiang. Palaeogeogr. Palaeoclimatol. Palaeoecol. 572, 110407.

Jiang, Q.F., Ji, J.F., Shen, J., Matsumoto, R., Tong, G.B., Qian, P., Ren, X.M., Yan, D.Z., 2013. Holocene vegetational and climatic variation in westerly-dominated areas of Central Asia inferred from the Sayram Lake in northern Xinjiang, China. Sci. China Earth Sci. 56, 339-353.

Jiang, Q.F., Meng, B.W., Wang, Z., Qian, P., Zheng, J.N., Jiang, J.W., Zhao, C., Hou, J.Z., Dong, G.W., Shen, J., Liu, W.G., Liu, Z.H., Chen, F.H., 2022. Exceptional terrestrial warmth around 4200-2800 years ago in Northwest China. Sci. Bull. 67, 427-436.

Joussaume, S., Taylor, K.E., Braconnot, P.J.F.B., Mitchell, J.F.B., Kutzbach, J.E., Harrison, S.P., Prentice, I.C., Broccoli, A.J., Abe-Ouchi, A., Bartlein, P.J., Bonfils, C., 1999. Monsoon changes for 6000 years ago: results of 18 simulations from the paleoclimate modeling intercomparison project (PMIP). Geophys. Res. Lett. 26, 859-862.

Kang, S.G., Wang, X.L., Roberts, H.M., Duller, G.A., Song, Y.G., Liu, W.G., Zhang, R., Liu, X.X., Lan, J.H., 2020. Increasing effective moisture during the Holocene in the semiarid regions of the Yili Basin, central Asia: evidence from loess sections. Quat. Sci. Rev. 246, 106553.

Lee, M.K., Lee, Y.I., Lim, H.S., Lee, J.I., Yoon, H.I., 2013. Late Pleistocene-H olocene records from Lake Ulaan, southern Mongolia: implications for east Asian palaeomonsoonal climate changes. J. Quat. Sci. 28, 370-378.

Leroy, S.A., López-Merino, L., Tudryn, A., Chalié, F., Gasse, F., 2014. Late Pleistocene and Holocene palaeoenvironments in and around the middle Caspian basin as reconstructed from a deep-sea core. Quat. Sci. Rev. 101, 91-110.

Leroy, S.A.G., Ricketts, R.D., Rasmussen, K.A., 2021. Climatic and limnological changes 12,750 to 3600 years ago in the Issyk-Kul catchment, Tien Shan, based on palynology and stable isotopes. Quat. Sci. Rev. 259, 106897.

Leroy, S.A.G., Lopez-Merino, L., Tudryn, A., Chalie, F., Gasse, F., 2014. Late

Pleistocene and Holocene palaeoenvironments in and around the middle Caspian basin as reconstructed from a deep-sea core. Quat. Sci. Rev. 101, 91-110.
Li, J.J., 1990. The patterns of environmental changes since last Pleistoc ene in northwestern China. Quat. Sci. 3, 197-204 (in Chinese with English abstract).
Li, X.Q., Zhao, K.L., Dodson, J., Zhou, X.Y., 2011. Moisture dynamics in central Asia for the last 15 kyr: new evidence from Yili Valley, Xinjiang, NW China. Quat. Sci. Rev. 30, 3457-3466.
Li, Y., Song, Y.G., Kaskaoutis, D.G., Zan, J.B., Orozbaev, R., Tan, L.C., Chen, X.L., 2021. Aeolian dust dynamics in the Fergana Valley, Central Asia, since~ 30 ka inferred from loess deposits. Geosci. Front. 12, 101180.
Li, Y., Song, Y.G., Orozbaev, R., Dong, J.B., Li, X.Z., Zhou, J., 2020a. Moisture evolution incentral Asia since 26 ka: insights from a Kyrgyz loess section, western tian Shan. Quat. Sci. Rev. 249, 106604.
Li, Y., Peng, S., Liu, H., Zhang, X., Ye, W., Han, Q., Zhang, Y., Xu, L., Li, Y.C., 2020b. Westerly jet stream controlled climate change mode since the Last Glacial Maximum in the northern Qinghai-Tibet Plateau. Earth and Planetary Science Letters, 549, 116529.
Lioubimtseva, E., 2014. Impact of Climate Change on the Aral Sea and its Basin. The Devastation and Partial Rehabilitation of a Great Lake, The Aral Sea, pp. 405-427.
Liu, X.Q., Shen, J., Wang, S.M., Wang, Y.B., Liu, W.G., 2007. Southwest monsoon changes indicated by oxygen isotope of ostracode shells from sediments in Qinghai lake since the late glacial. Chin. Sci. Bull. 4, 109-114.
Liu, X.K., Liu, J.B., Shen, C.C., Yang, Y., Chen, J.H., Chen, S.Q., Wang, X.F., Wu, C.C., Chen, F.H., 2020. Inconsistency between records of δ^{18}O and trace element ratios from stalagmites: evidence for increasing midelate Holocene moisture in arid central Asia. Holocene 30, 369-379.
Lorenz, E.N., 1956. Empirical orthogonal function and statistical weather prediction. Scientific Report No. 1 Statist Forecasting Project. Department of Meteorology, Massachusetts Institute of Technology.
Manoj, M.C., Srivastava, J., Uddandam, P.R., Thakur, B., 2020. A 2000 year multiproxy evidence of natural/anthropogenic influence on climate from the southwest coast of India. J. Earth Sci. 31, 1029-1044.
Mantua, N.J., Hare, S.R., 2002. The Pacific Decadal Oscillation. J. Oceanogr. 58, 35-44.
Mischke, S., Lai, Z.P., Aichner, B., Heinecke, L., Makhmudov, Z., Kuessner, M.L., Herzschuh, U., 2017. Radiocarbon and optically stimulated luminescence dating of sediments from Lake Karakul, Tajikistan. Quat. Geochronol. 41, 51-61.
Nagashima K, Tada R, Tani A, et al. 2011. Millennial-scale oscillations of the westerly jet path during the last glacial period. Journal of Asian Earth Sciences. 40 1214-1220. https://doi.org/10.1016/j.jseaes.2010.08.010.
Peltier, W.R., 2004. Global glacial isostasy and the surface of the ice-age Earth: The ICE-5G (VM2) model and GRACE. Annu. Rev. Earth Planet. Sci. 32, 111-149.
Peng, D., Zhou, T., 2017. Why was the arid and semiarid North-west China getting wetter in the recent decades? J. Geophys. Res. Atmos. 122, 9060-9075.

Ran, M., Feng, Z.D., 2014. Variation in carbon isotopic composition over the past ca. 46,000 yr in the loessepaleosol sequence in central Kazakhstan and paleoclimatic significance. Org. Geochem. 73, 47-55.
Randall, D.A., Wood, R.A., Bony, S., Colman, R., Taylor, K.E., 2007. Climate models and their evaluation. In Climate change 2007: The physical science basis. Contribution of Working Group I to the Fourth Assessment Report of the IPCC (FAR) (pp. 589-662). Cambridge University Press.
Rayner, N. A. A., Parker, D. E., Horton, E. B., Folland, C. K., Alexander, L. V., Rowell, D. P., Kent, E.C., 2003. Global analyses of sea surface temperature, sea ice, and night marine air temperature since the late nineteenth century, J. Geophys. Res. Atmos. 108, 4407.
Ren, Y., Yu, H., Liu, C., He, Y., Huang, J., Zhang, L., Hu, H., Zhang, Q., Chen, S., Liu, X., Zhang, M., Wei, Y., Yang, Y., Fan, W., Zhou, J., 2021. Attribution of Dry and Wet Climatic Changes over Central Asia. J. Clim. 35,1399-1421.
Ricketts, R.D., Johnson, T.C., Brown, E.T., Rasmussen, K.A., Romanovsky, V.V., 2001. The Holocene paleolimnology of Lake Issyk-Kul, Kyrgyzstan: trace element and stable isotope composition of ostracodes. Palaeogeogr. Palaeoclimatol. Palaeoecol. 176, 207-227.
Rotstayn, L., Collier, M., Dix, M., Feng, Y., Gordon, H., O'Farrell, S., Smith, I., Syktus, J., 2010. Improved simulation of Australian climate and ENSO-related climate variability in a GCM with an interactive aerosol treatment. Int. J. Climatol. 30, 1067-1088.
Rudaya, N., Tarasov, P., Dorofeyuk, N., Solovieva, N., Kalugin, I., Andreev, A., Daryin, A., Diekmann, B., Riedel, F., Tserendash, N., Wagner, M., 2009. Holocene environments and climate in the Mongolian Altai reconstructed from the Hoton-Nur pollen and diatom records: a step towards better understanding climate dynamics in Central Asia. Quat. Sci. Rev. 28, 540-554.
Schmidt GA, Kelley M, Nazarenko L, Ruedy R, Russell GL, Aleinov I, Bauer M, Bauer SE, Bhat MK, Bleck R, Canuto V, Chen YH, Cheng Y, Clune TL, Genio AD, de Fainchtein R, Faluvegi G, Hansen JE, Healy RJ, Kiang NY, Koch D, Lacis AA, LeGrande AN, Lerner J, Lo KK, Matthews EE, Menon S, Miller RL, Oinas V, Oloso AO, Perlwitz JP, Puma MJ, Putman WM, Rind D, Romanou A, Sato M, Shindell DT, Sun S, Syed RA, Tausnev N, Tsigaridis K, Unger N, Voulgarakis A, Yao MS, Zhang JL. 2014. Configuration and assessment of the GISS ModelE2 contributions to the CMIP5 archive. Journal of Advances in Modeling Earth Systems. 6, 141-184.
Sun, A., Feng, Z., Ran, M., Zhang, C., 2013. Pollen-recorded bioclimatic variations of the last ~22,600 years retrieved from Achit Nuur core in the western Mongolian Plateau. Quat. Int. 311, 36-43.
Tao, S.C., An, C.B., Chen, F.H., Tang, L.Y., Wang, Z.L., Lü, Y.B., Li, Z.F., Zheng, T.M., Zhao, J.J., 2010. Pollen-inferred vegetation and environmental changes since 16.7 ka BP at Balikun Lake, Xinjiang. Chin. Sci. Bull. 55, 2449-2457.
Tian, F., Herzschuh, U., Telford, R. J., Mischke, S., Van der Meeren, T., Krengel, M., 2014. A modern pollen-climate calibration set from central‐western Mongolia

https://doi.org/10.5194/cp-2023-71
Preprint. Discussion started: 15 September 2023

and its application to a late glacial-Holocene record. J. Biogeogr. 41, 1909-1922.

Tierney, J.E., Poulsen, C.J., Montañez, I P et al., 2020. Past climates inform our future. Science, 370(6517), 3701–3709.

Tierney, J.E., Poulsen, C.J., Montañez, I.P., Bhattacharya, T., Feng, R., Ford, H.L., Hönisch, B., Inglis, G.N., Petersen, S.V., Sagoo, N., Tabor, C. R., Thirumalai, K., Zhu, J., Burls, N.J., Foster, G.L., Goddéris, Y., Huber, B.T., Ivany, L.C., Turner, S., Lunt, D.J., Mcelwain, J.C., Mills. B.J.W., Otto-Bliesner, B.L., Ridgwell, A., Zhang, Y., 2020. Past climates inform our future. Science, 370, eaay3701.

Voldoire, A., Sanchez-Gomez, E., Mélia, D.S.Y., Decharme, B., Cassou, C., Sénési, S., et al. 2013. The CNRM-CM5.1 global climate model: Description and basic evaluation. Clim. Dyn. 40, 2091-2121.

Wang, B., Liu, J., Kim, H.J., Webster, P.J., Yim, S.Y., 2012. Recent change of the global monsoon precipitation (1979-2008). Clim. Dyn. 39, 1123-1135.

Wang, L., Jia, J., Xia, D, Liu, H., Gao, F., Duan, Y., Wang, Q., Xie, H., Chen, F., 2018. Climate change in arid central Asia since MIS 2 revealed from a loess sequence in Yili Basin, Xinjiang, China. Quat. Int. 502, 258-266.

Wang, P., Wang, B., Cheng, H., Fasullo, J., Guo, Z., Kiefer, T., Liu, Z., 2017. The global monsoon across time scales: Mechanisms and outstanding issues. Earth Sci. Rev. 174, 84-121.

Wang, Y.J., Cheng, H., Edwards, R.L., An, Z.S., Wu, J.Y., Shen, C.C., Dorale, J.A., 2001. A high-resolution absolute-dated late Pleistocene monsoon record from Hulu cave, China. Science 294, 2345-2348.

Wang, Q., Wei, H.T., Khormali, F., Wang, L.B., Xie, H.C., Wang, X., Huang, W., Chen, J.H., Chen, F.H., 2020. Holocene moisture variations in western arid central Asia inferred from loess records from NE Iran. G-cubed 21, e2019GC008616.

Watanabe, S., Hajima, T., Sudo, K., Nagashima, T., Takemura, T., Okajima, H., Nozawa, T., Kawase, H., Abe, M., Yokohata, T., Ise, T., Sato, H., Kato, E., Takata, K., Emori, S., Kawamiya, M., 2011. MIROC-ESM 2010: model description and basic results of CMIP5-20c3m experiments. Geoscientific Model Development. 4, 845-872,

Wei, W., Zhang, R., Wen, M., Yang, S., 2017. Relationshipbetween the Asian westerly jet stream and summer rainfall over Central Asia and North China: roles of the Indian mon-soon and the south Asian high. J. Clim. 30, 537-552.

Wu, P., Ding, Y., Liu, Y., Li, X., 2019. The characteristics of moisture recycling and its impact on regional precipitation against the background of climate warming over Northwest China. Int. J. Climatol. 39, 5241-5255.

Xie, C.Y., Li, M.J., Zhang, X.Q., 2014. Characteristics of summer atmospheric water resources and its causes over the Tibetan plateau in recent 30 years. J. Nat. Resour. 29, 979-989.

Xu, H., Lan, J., Zhang, G., Zhou, X., 2019. Arid Central Asia saw mid-Holocene drought. Geology 47, 255-258.

Yang, Y.P., Feng, Z.D., Zhang, D.L., Lan, B., Ran, M., Wang, W., Sun, A.Z., 2021. Holocene hydroclimate variations in the eastern Tianshan Mountains of northwestern China inferred from a palynological study. Palaeogeogr. Palaeoclimatol. Palaeoecol. 564, 110184.

Yu, G., Xue, B., Wang, S.M., et al., 2000. Chinese lakes records and the climate significance during Last Glacial Maximum. Chin. Sci. Bull. 45, 250-255 (in Chinese with English abstract).
Yukimoto, S., Adachi, Y., Hosaka, M., Sakami, T., Yoshimura, H., Hirabara, M., Tanaka, T.Y., Shindo, E., Tsujino, H., Deushi, M., 2012. A new global climate model of the Meteorological Research Institute: MRI-CGCM3: Model description and basic performance. J. Meteorol. Soc. Japan. 90, 23-64.
Zhang, H.L., Yu, K.F., Zhao, J.X., Feng, Y.X., Lin, Y.S., Zhou, W., Liu, G.H., 2013. East Asian Summer Monsoon variations in the past 12.5 ka: High-resolution δ18O record from a precisely dated aragonite stalagmite in central China. J. Asian Earth Sci. 73, 162-175.
Zhang, J., Nottebaum, V., Tsukamoto, S., Lehmkuhl, F., Frechen, M., 2015. Late Pleistocene and Holocene loess sedimentation in central and western Qilian Shan (China) revealed by OSL dating. Quat. Int. 372, 120-129.
Zhang, J.C., Lin, Z.G., 1992. Climate of China. Wiley, New York.
Zhang, D.L., Chen, X., Li, Y.M., Ran, M., Yang, Y.P., Zhang, S.R., Feng, Z.D., 2020. Holocene moisture variations in the arid central Asia: new evidence from the southern Altai mountains of China. Sci. Total Environ. 735, 139545.
Zhang, D.L., Feng, Z.D., 2018. Holocene climate variations in the Altai Mountains and the surrounding areas: a synthesis of pollen records. Earth Sci. Rev. 185, 847-869.
Zhang, Q., Lin, J., Liu, W., Han, L., 2019. Precipitation seesaw phenomenon and its formation mechanism in the eastern and western parts of Northwest China during the flood season. Sci. China Earth Sci. 62, 2083-2098.
Zhao, Y., An, C., Mao, L., Zhao, J., Tang, L., Zhou, A., Li, H., Dong, W., Duan, F., Chen, F., 2015. Vegetation and climate history in arid western China during MIS2: New insights from pollen and grain-size data of the Balikun Lake, eastern Tien Shan. Quat. Sci. Rev. 126, 112-125.
Sorg, A., Bolch, T., Stoffel, M., Solomina, O., Beniston, M., 2012. Climate change impacts on glaciers and runoff in Tien Shan (Central Asia). Nat Clim Change. 2, 725-731.
Zhang, D.L., Feng, Z.D., 2018. Holocene climate variations in the Altai Mountains and the surrounding areas: A synthesis of pollen records. Earth Sci Rev. 185, 847-869.